Current profile analysis and extreme value prediction in the LH11-1 oil field of the South China Sea based on prototype monitoring

Ming Liu[1], Wenhua Wu[1, 2, 5], Da Tang[3], Hongyan Ma[1], Arvid Naess[4]

1. Department Mechanics Engineering, Faculty of Vehicle and Mechanics, Dalian University of Technology, Dalian 116023, Liaoning, China
2. State Key Laboratory of Structural analysis for Industrial Equipment, Dalian University of Technology, Dalian 116023, Liaoning, China
3. Department of Computer Science and Technology, Dalian University of Technology, Dalian 116024, China
4. Dept. of Mathematical Sciences and Centre for Ships and Ocean Structures (CeSOS), Norwegian Univ. of Science and Technology, Trondheim, Norway.
5. Corresponding Author

Submitted for Publication to:
OCEAN ENGINEERING

Initial submission: June 2017

Revision: Nov 2017

Abstract: Current is a key ocean-environmental factor and exhibits strong non-stationary random characteristics. The complexities of current modeling present significant challenges for deep sea oil exploitation. The multiyear return period extreme current model is one of the key factors for the reliable design of marine structures. Recently, due to limitations of design specifications and guidelines, improved methods to predict extreme values for the South China Sea based on prototype monitoring are required. In contrast to the traditional extreme value analytical method, the newly developed Average Conditional Exceedance Rate (ACER) method is robust and shows good accuracy for estimations of ocean environmental loading. The method offers good reliability for short-term prototype monitoring data. This study performs multiyear return period extreme value prediction of the current profile based on prototype monitoring data collected in the Liuhua (LH11-1) oil field that was recorded by an in-situ monitoring system. The 1-year and 10-year return period current velocity design indexes were obtained using the ACER method. The present current velocity profiles of multi-year return periods were compared with two design current load indexes of two floating platforms in Liuhua area. The consistency with comparison to TLP platform design indexes shows that the ACER method provides the accuracy and flexibility of the results needed in the construction of current load models in the South China Sea. These results could provide the basis and reference for the design of offshore structure.

Keywords: South China Sea; current; profile characteristic; prototype monitoring; ACER; extreme prediction

1. Introduction

Although the South China Sea is rich in oil and gas resources with great exploration value, development of the deep-water fields is faced with significant challenges and uncertainty due to difficult observation and prediction of main environmental loads like wind, wave, and current. The ocean current has become a major load factor in the structural design of offshore oil and gas exploitation equipment, especially for use in deep-water regions. There are several influences of ocean current on offshore engineering structures. First, a large drag force will be generated on the structure under the effect of high-velocity current, causing strong resistance for towing and positioning. This can cause the tension in the anchoring and riser system of the platform to exceed acceptable limits. Second, VIV (Vortex Induced Vibration) of pipes will be generated in addition to the interaction of drag force, when the ocean current flows through the middle part of the riser. This long-term VIV will bring about fatigue failure to the riser. For these reasons, a study of the current distribution is critical to solve the load problem in the design of offshore engineering structure in the deep sea.

Many recent studies (He et al., 2012; Liu et al., 2002; Yang et al., 2013) have been performed to analyze ocean currents in the South China Sea. Numerous studies based on meteorological observations and ocean hydrological telemetering have been conducted with a main focus on the description of the regularity of observation results. However, extensive studies of the loading targeted for engineering applications are still in their preliminary stage. In general, prediction and analysis of current velocity of multiyear return periods are important to understand current loading for offshore engineering structures. To predict potential extreme values, extreme value theory and curve-fitting methods are usually adopted to determine the long-term distribution of offshore loads.

Then, an appropriate theoretical frequency curve can be determined by coordinate transformation and then extended to obtain the extreme value for multiyear return periods (Ma, 2006; Wang, 2005). Carollo et al. (2005) utilized GEV (Generalized Extreme Value) distribution and GPD (Generalized Pareto Distribution) to negotiate the vertical structure of current extreme values in the Faroe Bank channel and compared these methods to the FOAM (Forecasting Ocean Assimilation Model) numerical model. Jonathan et al. studied multivariate extreme value problems of ocean engineering including ocean current profile and wave height (Jonathan et al., 2010, 2012; Ewans and Jonathan, 2014) based on the model of multivariate conditional extreme value proposed by Heffernan and Tawn (2004). Dong (2009) adopted the Pearson Type Ⅲ distribution to calculate the extreme values of wind-driven currents at Bohai Gulf and determined the final extreme value distribution of currents with tide vectors. Ge et al. (2009) used a 3-parameter Weibull extreme value distribution based on numerical simulation and data assimilation to calculate the return values of wind, waves, and current in four representative deep-water areas of the South China Sea. These estimation methods of extreme values are empirical models, like experience frequency and Pearson type Ⅲ methods, or models based on extreme value theory, like Gumbel, Weibull, and the POT model (Chen, 1991). The latter is derived from the extreme value theory with a theoretical basis, and is widely used to determine the major distribution form of extreme values of ocean variables. And these methods are mostly based on asymptotic theory (Smith, 2002), where extreme value samples are assumed to comply with a particular form of asymptotic distribution. However, the distribution of samples is hard to predict in advance, and the applicability of the above prediction methods should be further improved. Recently, researchers have paid attention to the analysis of the interlayer inherent correlation of current profiles (Forristall and Cooper, 1997; Lima et al., 2009). But due to the difficulties such as modal losses,

linear assumptions, the research achievements are still limited. Prediction using current profile models by considering inherent correlation is still in the preliminary stage. The authors are studying the regularities of current distributions and the interlayer inherent correlation, and results from this work will be published in the future.

To overcome the indicated defects of traditional asymptotic extreme value prediction methods, Naess and Gaidai (2009) proposed a more flexible extreme value analysis method, the Average Conditional Exceedance Rate (ACER) method, which does not depend on traditional asymptotic extreme value theory. This method can adopt the forms of asymptotic distribution indirectly and maintain the asymptotic characteristics of the original data samples. This increases the accuracy of the prediction and reaches the asymptotic consistency of traditional extreme value theory. The ACER method was based on the average conditional exceedance rate function, or the mean upcrossing rate function in earlier time. In 2008, Naess and Gaidai utilized the mean upcrossing rate function to perform numerical simulation on the extreme value response of the dynamical system through Monte Carlo simulation with verification of universality and robustness of the method, greatly reducing calculation time. Next, they improved the original method using revised ARE functions to be applicable to a generalized time series and even a non-stationary random process (Naess and Gaidai, 2009). The random responses of narrow-band and dual peak spectra were utilized to carry out numerical verification of the ACER method, and the results indicated the reliability and accuracy of the ACER method (Naess et al., 2007, 2009, 2010). Karpa and Naess (2013) conducted extreme value predictions of wind speed samples from three observation stations in Coastal Norway through the ACER method and compared the results with results obtained from traditional Gumbel and POT

methods. The comparison showed that the ACER method provided better accuracy, stability, and insensitivity to anomalous points.

The design of offshore engineering equipment in China has always adopted API and DNV design criteria due to the lack of long-time prototype measured data. The specification of DNV NO. 30.5 has been adopted as the design basis of ocean environment loads (Veritas, 2000; NDRC, 2004). The specification provides a mechanical description of environmental conditions and environmental loads. However, the current load was presented as a general formula of drag force, unlike the more detailed descriptions of the wind and wave loads. Thus, the current load design basis and computational method has not yet been demonstrated clearly. The spatial distributions in existing specifications were obtained from beach and coastal areas. Due to the lack of applicability for the deep-water environment, it is insufficient to serve as an actual reference basis to define the current load for offshore engineering design. At the same time, current load models including international specifications were obtained based on data analysis of other sea regions. However, the applicability of these models must be verified due to the complexity of the South China Sea. Overall, it is essential to study current loads based on prototype data measured in the South China Sea. To address this need, the goal of this study was to investigate current loads at the LH 11-1 sea region based on the prototype monitoring system built by “NanHaiTiaoZhan" FPS and the ACER extreme value analysis method. In this paper, an ACER based extreme value prediction method was applied to predict the extreme current, and two design indexes are subsequently verified. The achievements of the current model for multiyear return periods can provide significant guidance for load selection and application in offshore engineering design, especially in the South China Sea.

2. Prototype monitoring of offshore engineering structure

Theoretical analysis, numerical simulation, and model testing are the main research methods applied to the design of offshore equipment structures. However, integral analysis of the structure of large offshore platform systems containing a variety of complex substructures cannot be conducted with full dependence on the theoretical analysis, derivation, and calculation. The inevitable simplifications of the structure may distort the analysis results. Numerical simulations include model approximation, linearization, decoupling calculation, and other processes of simplification that can produce large errors. Model testing is an essential aspect of offshore engineering equipment design, but there are limits due to complex real sea conditions. Limited by the size of the testing pool, truncation and scale effects are inevitable in the test. Designed to overcome the above defects of traditional methods, the prototype monitoring method aims to obtain the actual load and structural dynamic response through prototype testing under real sea conditions. Structural analysis based on data from prototype monitoring should be more reliable. Unfortunately, without enough data from prototype testing, only limited specifications and guides could be applied to offshore structural design in the South China Sea. For example, related specifications (NDRC, 2004) indicate that the following formula can be employed to calculate the gradient of current velocity if there is no available current data for a shallow ocean area (water depth less than 150 m).

$$V_c = V_T\left(\frac{y}{H}\right)^{\frac{1}{7}} + V_W\left(\frac{y}{H}\right). \tag{1}$$

where, V_T is the current velocity of the tide, V_W is the velocity of the wind-driven current, y is the depth from the ocean bottom, and H is the water depth. However, the computation of Eq. (1) is complex, especially when it is generally difficult to obtain actual values of V_T or V_W. Additionally, the

formula is only valid for the estimation of currents in shallow water, but not the actual current load distribution in deep water or a complex sea region. Therefore, it has become increasingly important to analyze the current model using prototype monitoring.

2.1 The prototype monitoring system of the "NanHaiTiaoZhan" FPS (NHTZ FPS)

The NHTZ FPS is a semi-submersible drilling platform serving the LH11-1 oil field (Fig. 1 and Fig. 2) in the South China Sea. It has a weight of 16735 tons, total length of 90 meters, molded breadth of 75 meters, molded depth of 40 meters, and total height of 110 meters. In this region of the LH11-1 oil field, the water depths range from 260 m to 300 m (Qu et al., 2013).

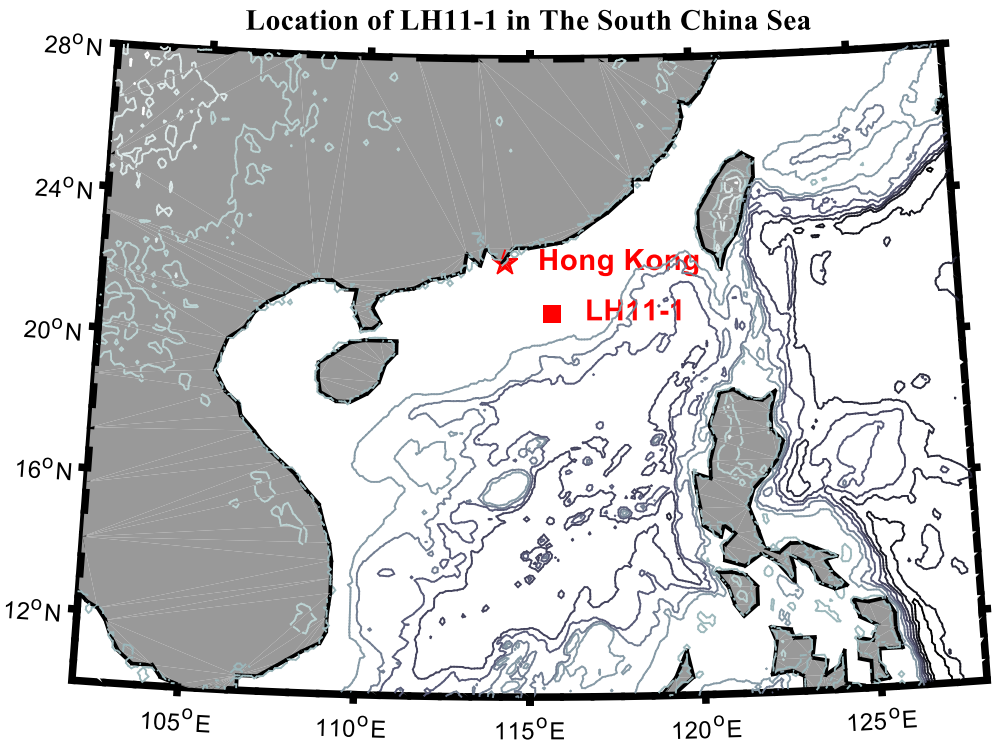

Fig. 1 LH11-1 geographical position

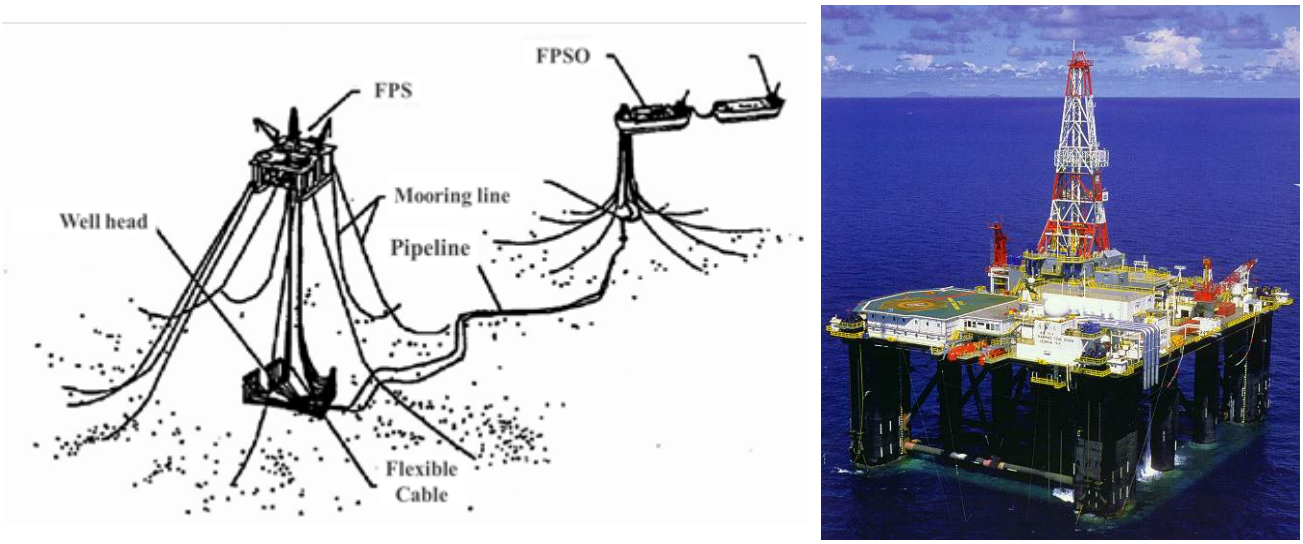

Fig. 2 LH11-1 oil-gas field exploration mode and the semi-submersible platform of the NHTZ FPS

A prototype monitoring system has been designed, implemented, and installed on NHTZ FPS, to measure comprehensive environmental loads and structural dynamic response (Du et al., 2016; Wu et al., 2013; Yuan, 2013). Prototype data can be used for guidance in structural design, safety assessment, and platform operation. The prototype monitoring system (as shown in Fig. 3) is mainly composed of a power supply system, a network system, an environmental collection system, and a response collection system. This system can collect environmental and structural response data using an individual power supply system even under extreme weather, like a typhoon. In this study, long-term prototype monitoring data were utilized for ocean current analysis.

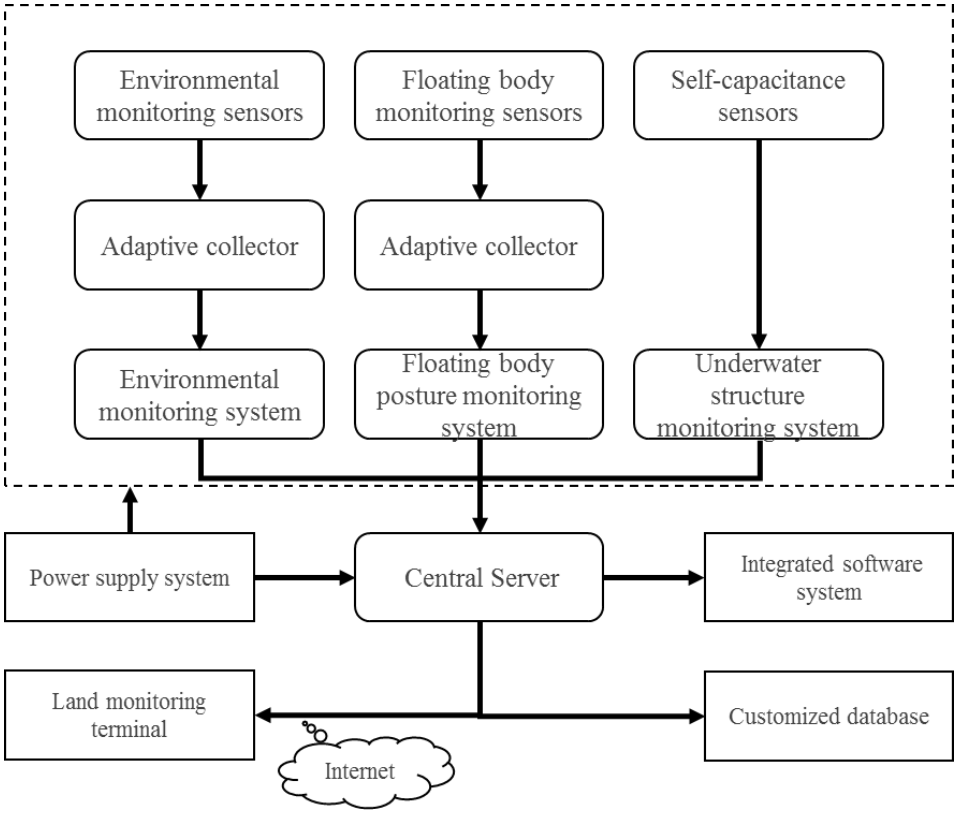

Fig. 3 The prototype monitoring system of the NHTZ FPS

2.2 Overview of prototype monitoring scheme of the ocean current

The NHTZ FPS is located in deep water in the LH 11-1 oilfield, and here typhoons and harsh sea states are frequent. Directly affected by the northeast monsoon and offshore forcing (Kuroshio intrusion), this sea area has strong wind, high waves, and fast current, part of the severest dynamic environment in the South China Sea (He et al., 2009). Two ADCP (Acoustic Doppler Current Profile) current gauges (Fig. 4) are deployed in the prototype monitoring system to measure the full current profile (including velocity and direction) in the surface and the deep-water, respectively. The current directions are defined clockwise from North. The surface current gauge was installed at depths between 15 and 20 m. The measuring range was divided into 12 layers along the water depth with an interval of 1 m and a sampling rate of 10 minutes. The deep-water current gauge was installed at

depths between 20 and 25 m. The measuring range (water depth about 150 m) was divided into 14 layers with an interval of 7 m and a sampling rate of 10 minutes. In this study, data measured from Jun. 3rd 2013 to Jul. 2nd 2015 were used to generate current profile analysis and predict the extreme values of multiyear return periods based on the ACER method. Fig. 5 shows characteristic data of the partial currents in the prototype monitoring procedure.

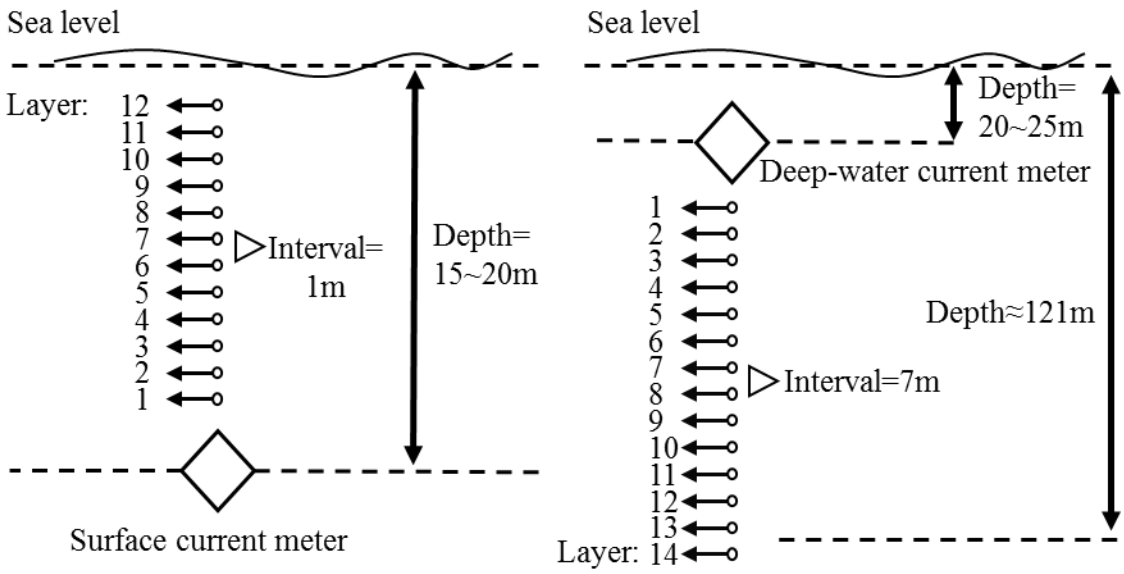

Fig. 4 Current gauges both on the surface and deep water measurement

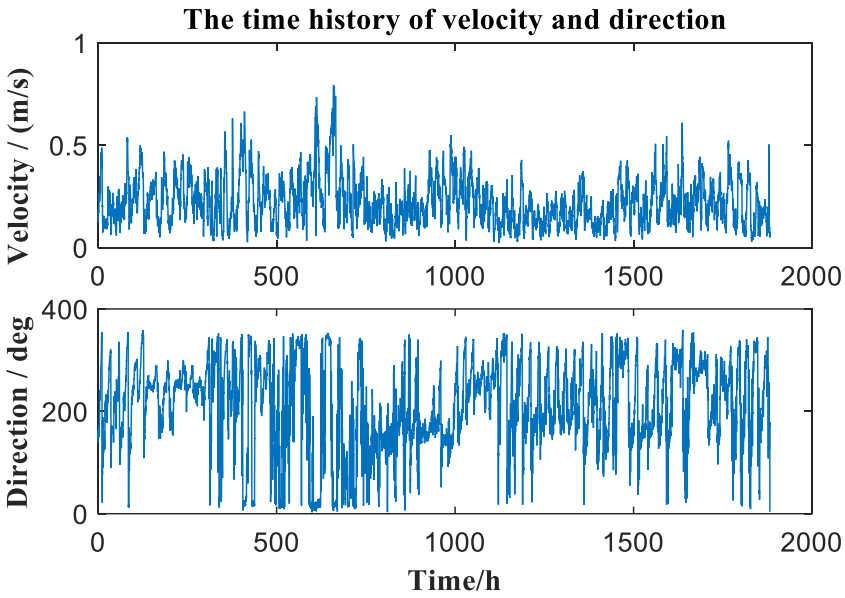

Fig. 5 Current data in the prototype monitoring system

3. Multiyear return period values and the ACER method

3.1 Sea condition in multiyear return period

The load condition of extreme offshore environments of a multiyear return period must be seriously considered in the design of an offshore engineering structure. Various structural failures are easy to trigger in such an extreme environment. Statistically, the multiyear return period value describes the average level of probability that the value can occur during the corresponding return period, and the return period is the average time interval in which a certain event occurs repeatedly. Estimation of the corresponding extreme sea conditions of a return period can be done when the distribution of the extreme values is known.

Assuming that the maximum value of a certain ocean environment factor during one year is x_M, its distribution function can be represented as F,

$$F(\eta) = Prob\{x_M \le \eta\} = \int_{-\infty}^{\eta} f(x)dx = p. \tag{2}$$

where, η is a particular threshold value of the ocean environment factor; p is the probability of the event $\{x_M < \eta\}$; and $f(x)$ is the probability density function of the distribution F. In general, the corresponding return period in years of η is defined as

$$T = \frac{1}{p'} = \frac{1}{1-p} \quad . \tag{3}$$

The extreme value distribution F and the return period T possess the following relationship:

$$F(\eta) = Prob\{x_M \le \eta\} = p = 1 - \frac{1}{T}, \tag{4}$$

where η corresponds to the extreme value level exceeded on the average once every T years.

3.2 Characteristics and advantages of the ACER method

The ACER method is a recently developed approach to analyze and predict extreme values. Naess et al. (2007, 2008, 2009, and 2010) conducted numerical verifications to validate the method for many extreme value responses of dynamic systems. The simulation results showed that the ACER method can be utilized for more accurate estimation of the extreme value distribution of sample data compared with traditional extreme value methods. When combined with the recommended extrapolation algorithm, the extrapolated results of the ACER method are insensitive to abnormal values and become more robust. Additionally, application of the procedure is simple and user-friendly. ACER is an effective diagnostic tool to evaluate the degree of correlation of time series data by the calculation and analysis of different ACER functions. Without requirements about independent data, the ACER method possesses universal applicability and can be used for extreme value analysis of time series for multiple random processes. The ACER method has been extended to practical applications for the prediction of extreme values of ocean environment variables like wind speed (Karpa and Naess, 2013), wave heights (Naess and Karpa, 2015) and sea water levels in coastal areas (Skjong et al., 2013). The successful applications of the ACER method suggest that the use of this system to analyze and predict current extreme values will be of great reference value.

3.3 Basic principle of the ACER method

The ACER method focuses on the relationship between the average conditional exceedance rate (or ACER functions) of a time series and a given threshold value η. In this way, the study of extreme value distributions can be skillfully converted into research on ACER functions.

The ACER function $\varepsilon_k(\eta)$ is defined as follows (Naess and Gaidai, 2010):

$$\varepsilon_k(\eta) = \frac{1}{N-k+1}\sum_{j=k}^{N}\alpha_{kj}(\eta), k = 1, 2, ... \quad (5)$$

where, N is the total number of samples in a given time series $(X_1, X_2, \quad X_j ..., X_N)$; k, a constant less than N, means that each sample point in the time series is assumed to depend only on the previous k-1 sample points; $\alpha_{kj}(\eta) = Prob(X_j > \eta \mid X_{j-1} \le \eta, ..., X_{j-k+1} \le \eta)$ is the conditional probability of the event when the jth sample point X_j exceeds the given threshold η while the previous $(k-1)$ sample points $(X_{j-1}, ..., X_{j-k+1})$ do not exceed this threshold. The event can be called a conditional exceedance event. Then, $\sum_{j=k}^{N}\alpha_{kj}(\eta)$ represents the mathematical expectation of the frequency of occurrence of the event, i.e. the expectation of conditional exceedances. In general, $\varepsilon_k(\eta)\cdot(N-k+1)$ equals the average number of conditional exceedances.

As described by Naess and Gaidai (2009), the ACER function and the extreme value distribution $F(\eta)$ possess the following relationship derived by the method called "Cascade of conditioning approximations".

$$F(\eta) \approx \exp\left(-\left(N-k+1\right)\varepsilon_k\left(\eta\right)\right), (\eta \to \eta_{\text{extreme}}, k \to k_c), \quad (6)$$

where, η_{extreme} is noted as extreme value, k_c an appropriate value of k. For the kth-order cascade of conditioning approximations, the right side of the equation (6) will converge to the correct extreme value distribution when $k \le N$ is large enough. For the cascade of approximations to have practical significance, it should be verified that the property $k = k_c << N$ is indeed satisfied for the data analyzed. The appropriate k to choose to account for dependence in the time series will be clearly revealed by the plot of the estimated ACER functions that will be presented in section 4.2.1. Since the focus is on the extreme levels, any function that provides correct estimates of the extreme distribution function at the extreme levels can be used. Therefore, the study of the extreme value distribution can be converted to direct analysis of the tail ($\eta \ge \eta_1$, η_1 is the truncation point or the tail

marker) of the ACER functions. Naess and Gaidai (2009) gave the following specific mathematical form for its truncated distribution:

$$\varepsilon_k(\eta) \approx q_k \exp\left\{-a_k(\eta - b_k)^{c_k}\right\}, \eta \geq \eta_1. \tag{7}$$

where a_k, b_k, c_k and q_k are constants. The current conditions for a multiyear return period can be calculated using the ACER functions when the above parameters have been determined. The following revised ACER functions are adopted in the actual calculation to perform empirical estimation considering a non-stationary random process, cf. Karpa and Naess (2013). The revised ACER function is presented as:

$$\varepsilon_k(\eta) = \frac{\sum_{j=k}^{N} E\left[A_{kj}(\eta)\right]}{N-k+1} \tag{8}$$

where, A_{kj} is the indicator function of conditional exceedance event, meaning that $A_{kj} = 1$ when a conditional exceedance event occurs. $E(\ )$ denotes the expectation operator. For more than one sample of time series, the empirical estimation is as follows:

$$\begin{cases} F(\eta) \approx \exp\left(-(N-k+1)\hat{\varepsilon}_k(\eta)\right), \\ \hat{\varepsilon}_k(\eta) = \dfrac{1}{R}\sum_{r=1}^{R} \hat{\varepsilon}_k^{(r)}(\eta), \\ \hat{\varepsilon}_k^{(r)}(\eta) = \dfrac{1}{N-k+1}\sum_{j=k}^{N} a_{kj}^{(r)}(\eta). \end{cases} \tag{9}$$

where, the total amount of samples is represented as R; each sub-sample is represented as r; $a_{kj}^{(r)}$ is realizations in each sub-sample corresponding to $A_{kj}^{(r)}$, representing whether the j th point is exceeding η; the value of $a_{kj}^{(r)}$ is also obtained as 1 or 0; and $\hat{\varepsilon}_k(\eta)$ is the ACER function obtained by the empirical estimation. After empirical estimation, $\hat{\varepsilon}_k(\eta)$ needs to be fitted by (7), which can be transformed into a linear regression problem by coordinate transformation to obtain a solution by

application of the constrained Levenberg-Marquardt least squares optimization method. The main algorithm of the optimization process is as follows.

The objective function is

$$F_{obj}\left(a,b,c,q\right)=\sum_{i=1}^{n}w_i^{'}\left(\log\varepsilon_k\left(\eta_i\right)-\log q+a\left(\eta_i-b\right)^c\right)^2. \tag{10}$$

where the weight factor $w_i^{'}=w_i/\sum_{j=1}^{n}w_j$ and $w_i=\left[\log CI^{+}\left(\eta_i\right)-\log CI^{-}\left(\eta_i\right)\right]^{-2}$; CI^{+} and CI^{-} correspond to the upper and the lower limits of the confidence interval for $\hat{\varepsilon}_k\left(\eta\right)$, and they are expressed as follows:

$$CI^{\pm}\left(\eta\right)=\varepsilon_k\left(\eta\right)\pm\tau\cdot s_k\left(\eta\right)/\sqrt{R}, \tag{11}$$

in which $\hat{s}_k$ is the standard deviation of $\hat{\varepsilon}_k(\eta)$ and $\tau=t^{-1}((1-0.95)/2,R-1)$ is the corresponding quantile of the student's *t*-distribution with *R*-1 degrees of freedom.

In case only one realization is available, the way to estimate a confidence interval is to assume that the number of conditional exceedances $\varepsilon_k(\eta)\cdot(N-k+1)$ follows the Poisson distribution, which asymptotically is Gaussian distribution. Therefore, an approximate confidence interval of $\hat{\varepsilon}_k(\eta)$, and also $\varepsilon_k(\eta)$, can be written as (Karpa and Naess, 2013)

$$CI^{\pm}(\eta)=\hat{\varepsilon}_k(\eta)(1\pm\nu/\sqrt{(N-k+1)\hat{\varepsilon}_k(\eta)}). \tag{12}$$

where ν is the corresponding quantile of the Gaussian distribution. Then, the procedure of the parameter optimizing algorithm can be presented as:

$$\begin{cases} F_{obj}\left(a,b,c,q\right)\rightarrow\min, \\ \log q-a\left(\eta_i-b\right)^c\le 0, i=1,\ldots,n, \\ \left\{a,b,c,q\right\}\in S, \\ S=\left\{\left\{a,b,c,q\right\}\in\ \ ^4\,|\,a,c,q\in\left(0,+\infty\right);b\in\left[0,\eta_1\right]\right\}. \end{cases} \tag{13}$$

The inequality constraint in the above formula is because $\hat{\varepsilon}_k^{(r)}(\eta) = 1/(N-k+1)\sum_{j=k}^{N}\alpha_{kj}^{(r)}(\eta)$ is satisfied in the empirical estimation of the ACER functions. Thus, $\hat{\varepsilon}_k(\eta) = \frac{1}{R}\sum_{r=1}^{R}\hat{\varepsilon}_k^{(r)}(\eta) \le 1$ and $\log \hat{\varepsilon}_k(\eta_i) \le 0$.

That is, the left side of the inequality should be less than or equal to 0 and S is the restricted domain where the four constants (a, b, c, q) will be determined.

By the previous discussion, we can see that the original time series can be directly analyzed through the ACER method. In this way, the complex process and the problem of insufficient samples due to extraction of extreme value samples from the original (for example short-term period) measured data can be avoided for the non-narrow-band random process. For the actual application, empirical estimations should first be conducted on ACER functions for different k values by (5) or (9). Among these empirical estimations, simply select one of them to perform the optimal fitting of the curve (7). The details are discussed in section 4.2.1. Then, the tail marker η_1 needs to be determined to carry out optimal fitting of the curve to obtain ACER functions by combining Eq. (10) with Eq. (13). Finally, the extreme value of multiyear return periods of the ocean current can be deduced using ACER functions as shown by Eq. (6), which describes the relationship of the distribution of extreme values and ACER functions. Moreover, an optimal confidence interval will be significant for quantifying the uncertainty on ACER function. For estimation of the optimal confidence interval, the empirical confidence band from measurement data is first reanchored to the fitted optimal curve. Then the optimal curve fitting procedure is applied to the reanchored confidence band to determine a final optimal confidence interval band. The confidence interval of the predicted return value can therefore be obtained from the extrapolated optimal confidence interval band. This procedure seems to give confidence intervals that are consistent in length but slightly shifted

compared with the results obtained by a non-parametric bootstrapping method (Karpa and Naess, 2013).

4. Profile distribution analysis and prediction of the extreme value of the prototype monitoring current

4.1 Distribution of current profile

The prototype monitoring system of NHTZ FPS acquires the long-term current profile data by ADCP gauges for the LH11-1 sea area. Here, current profile data measured in the deep water were selected for analysis and prediction of the extreme value to avoid the effects of waves on surface current.

In general, the analysis of extreme values of wind, current, and other factors ignore the effect of direction. For example, current direction is neglected when analyzing the reliable design of a riser, such as VIV. Similarly, current direction is not considered in this paper. For further research in the future, related published work (e.g. Robinson and Tawn 1997, Jonathan et al. 2012) can provide significant support and references. Figure 6 presents several representative velocity profile distributions from prototype measurements. It can be seen that the current velocity profile is complex, exhibiting different spatial shapes in different periods. The trend is not obvious at times, although the upper current velocity is larger than the lower one in most cases. It should be noted that the current velocity of the middle-depth profile (8 to 10 layers, 86 to 100 meters) is obviously lower than that of the upper and bottom layers (Figure 6 c), during some periods of our observation. In this case, the current velocity profile decreases initially and then increases with increased water depth with a long duration.

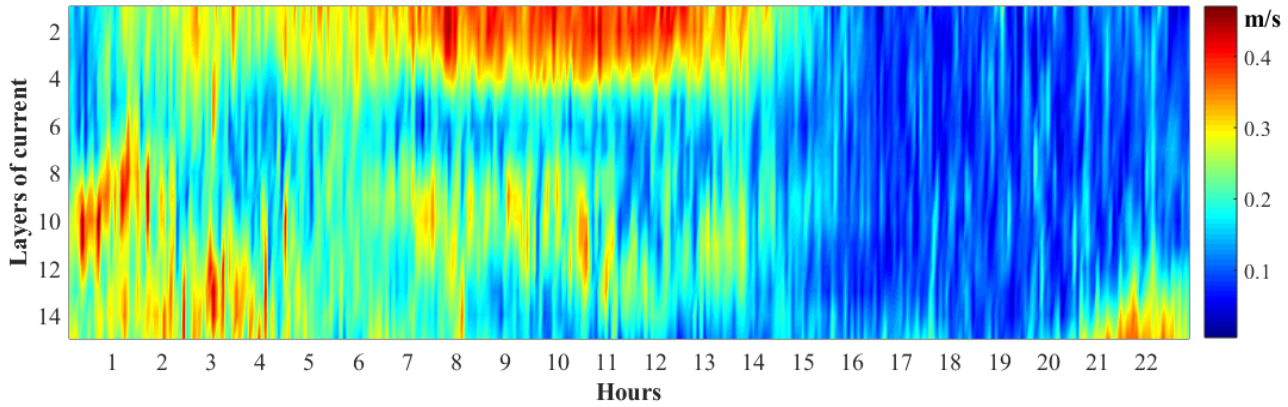

Fig.6a

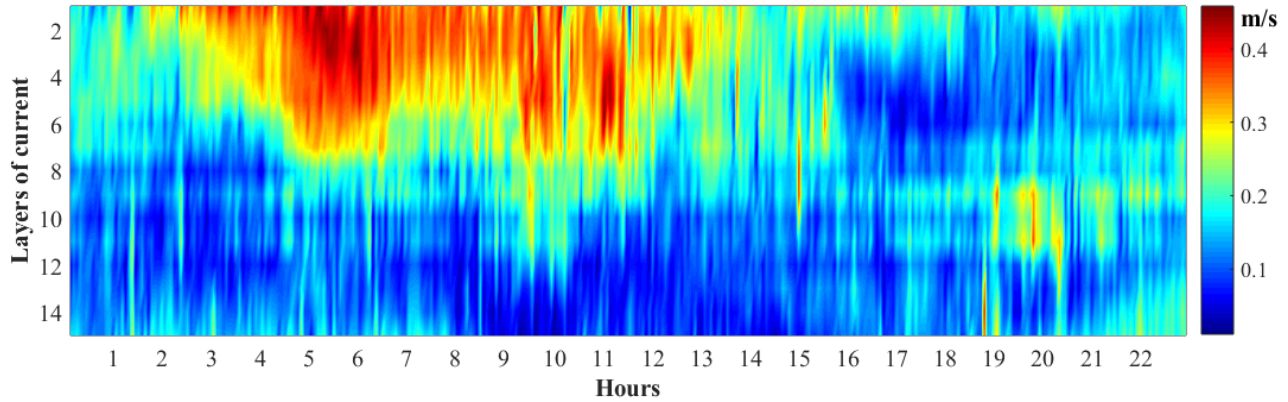

Fig.6b

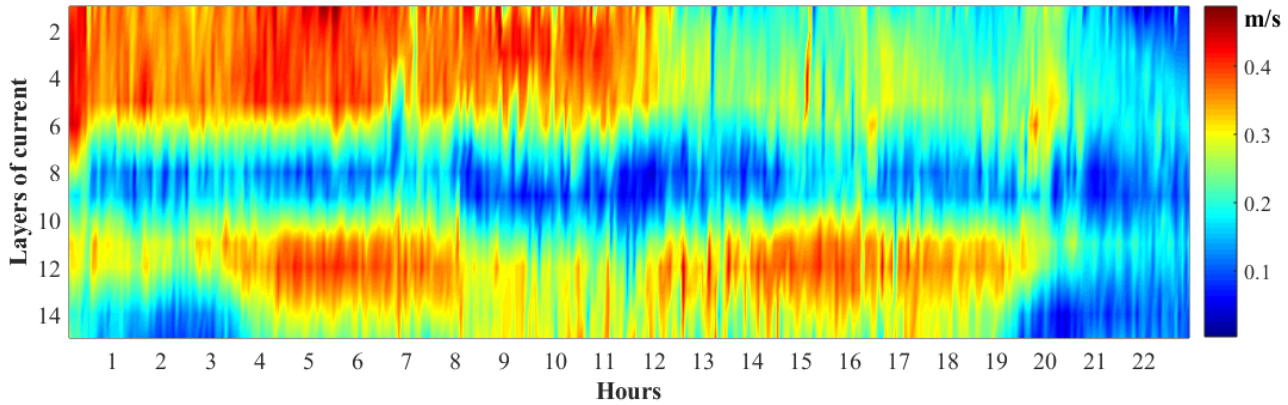

Fig.6c

Fig. 6 Distribution of typical profile current velocity

Figure 7 shows the spatial distribution of the mean value of each layer of the velocity profile. Two vertical axes of coordinates are used to show the current layer of the mean profile with its corresponding depth. The 95% confidence interval is obtained by a nonparametric bootstrap method

with a sample size of 10000. Assuming that the mean value follows the normal distribution, the estimated confidence interval can be expressed by the following formula:

$$CI_{mean}^{\pm} = [v_m - 1.96 s_m^*, v_m + 1.96 s_m^*] \tag{14}$$

where v_m denotes the estimated mean velocity and s_m^* denotes the standard deviation of the mean velocity. As shown in Fig.7, the mean profile and attached 95% confidence interval are marked with solid and dashed lines respectively.

Similarly, the small current velocity distribution behavior can also be detected in some parts of the middle-lower layers (marks indicated with red dashed lines). The overall spatial distribution of the mean velocity value displays a shear flow characteristic. The mean values of the upper and lower layers changed slightly with depth. The mean velocity value of middle layer changed obviously with increased depth and a large gradient.

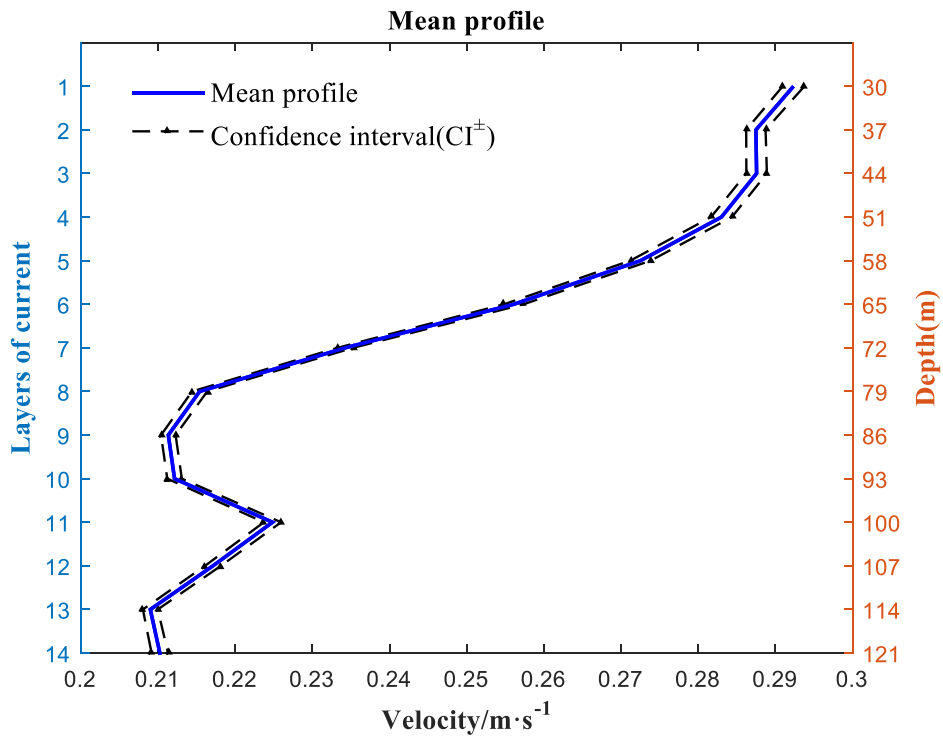

Fig. 7 Mean values of current velocity profile

4.2 Prediction of the extreme value of current profile based on the ACER method

4.2.1 Empirical estimates of ACER functions for different water depths

Similar to *k*th-order Markov approximation, the *k* value at each sample point is assumed to rely only on the previous *k*-1 sample points. Hence, the determination of the *k* value in the ACER function depends on the inherent dependence of sample points in the original time series. The dependence can be clearly revealed by the plot of the estimated ACER functions. Taking the first layer of current data as an example, the plot of the empirically estimated ACER functions for *k* from 1 to 10 is presented in Fig.8. In order to facilitate the observation, Fig. 8 has been split into two subgraphs. Fig 8(a) aims to demonstrate the difference of the ACER functions. Fig 8(b) focuses on the zoom effects with $\eta \geq 0.8$ to explore the convergence of the tail ACER functions. The different values of *k*, corresponding to different ACER functions, represents the *k*th-order extreme value distribution approximation in Eq. (6). The *k* value should be increased until the ACER functions have converged, at least in the tail. As indicated in section 3.3, the right side of the Eq. (6) will converge to the extreme value distribution when $k(\leq N)$ is large enough. For our data, there is a clear indication that the ACER functions show asymptotic convergence in the tail. In this case, with $k \geq k_c$ as an example, the sample points can be assumed to be conditional on the previous *k*-1 sample points in extreme value analysis. In other words, the sample data used in the traditional POT method can be regarded as statistically independent when the sampling interval is more than k_c. On the other hand, the ACER method does not require independent data. That is, all the data are processed, and there is no need for initial declustering of the data. The ACER function of $k \geq k_c$, which extract the extreme value samples inherent, is enough and appropriate for further extreme analysis. Therefore, consistent extreme value analysis can be performed if the selected ACER function satisfy the asymptotic convergence condition. The ACER functions plot can help to reveal the dependence structure of the

current velocity in the time domain and can be regarded as a diagnostic tool to determine the value of k for consistent extreme value estimation.

As shown in Figure 8, ACER functions can be regarded as showing asymptotic convergence in the tail at least when $k \geq 6$ .The corresponding time interval $t = k \times \Delta t = 6 \times 10\,\text{min} = 1\text{h}$ (with a sampling interval $\Delta t = 10\,\text{min}$), thus the time series of current velocity show significant dependence of the 6 sample points in a one hour increment. When the sampling time interval exceeds 1 h, the sample data for the extreme value analysis can be considered independent. Here, the empirically estimated ACER function (as shown in Fig. 9) of k=8 is selected for the optimal curve fitting analysis.

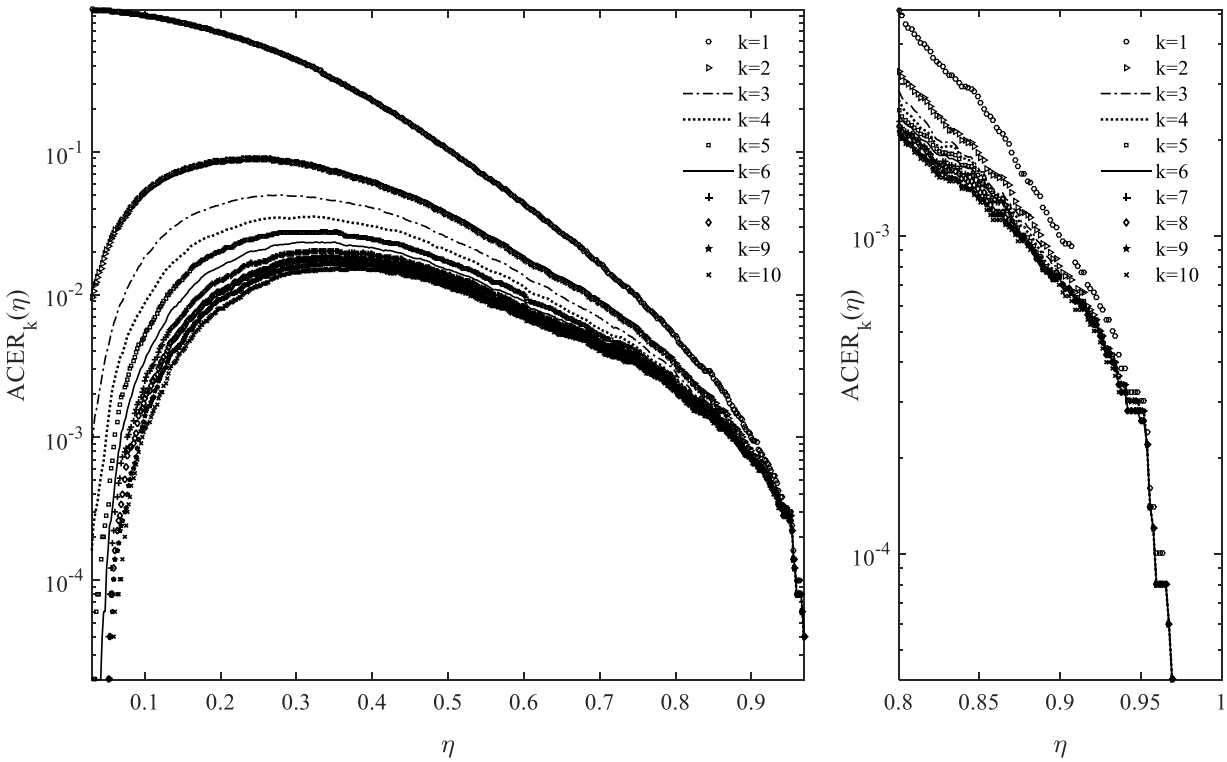

a. ACER functions with *k* from 1 to 10 **b. Tail ACER functions at *η*≥0.8**

Fig. 8 Empirical estimation of ACER functions for different *k* values

4.2.2 Determination of the optimal curve fitting parameters

The ACER function exhibits a decreasing trend with the increase of η. However, there will be a spurious peak in the non-stationary process when η is small. In general, ACER function focus more on the distribution behavior of the tail, so that the peak value should be neglected while selecting the truncated point (Tail Marker, i.e. η_1). On the other hand, overly large η_1 will cause insufficient tail data available for subsequent optimal fitting. Hence, we advise that η_1 should be slightly larger than the corresponding value of the peak. Moreover, it has been observed that the predicted return value is not very sensitive to the choice of η_1 (Naess and Gaidai, 2009).

Considering the fewer data points when η is big, there may be considerable uncertainty with low data reliability. The tail uncertainty δ can be measured by the relative confidence band width (Naess and Gaidai, 2009) according to Eq. (11) or (12). Eq. (12) is adopted here when only one realization of measured current is available. For high levels of η in the tail, an approximate 95% confidence interval of $\hat{\varepsilon}_k(\eta)$, and also $\varepsilon_k(\eta)$, can be written as

$$CI^{\pm}(\eta) = \hat{\varepsilon}_k(\eta)(1 \pm 1.96 / \sqrt{(N-k+1)\hat{\varepsilon}_k(\eta)}) . \tag{15}$$

Then, δ can be defined by the relative confidence band width as

$$\delta = 1.96 / \sqrt{(N-k+1)\hat{\varepsilon}_k(\eta)} \in (0.5,1) . \tag{16}$$

Quality control of the tail data (marked in dashed box of Fig. 9) can be realized by adjusting δ. For δ more than a certain value such as 0.6, corresponding tail data will be filtered out as outliers. This processing effects can differ for different data types. In the practical work, δ provides a limited control effect for the quality of the data under some conditions in the current velocity data process. Another pre-processing was conducted as follows in the tail part of the data before the calculation and processing described above. As shown in Fig. 10, the amount of tail data that should be prepared for pre-processing can be identified by the histogram and approximate probability

density curve. The tail data for which the probability density approaches zero will be removed. The one in a thousand upper quantile in the tail was selected as the criterion where the probability density functions of measured current velocity is assumed close to zero. Because a current velocity exceeding this criterion indicates a rare event in statistics and will be highly uncertain. As shown in Fig.10, that is 0.97, which is the one in a thousand upper quantile. And prototype monitoring data larger than the corresponding value were first removed and then the quality control of the tail data could be realized sequentially by δ.

Once quality control is finished, the optimal curve fitting described in Eq. (13) can work quite well by the Levenberg-Marquardt least-squares optimization method combined with the objective function in Eq. (10). The extreme value of multiyear return periods of the ocean current can be extrapolated based on an assumed tail behavior of the ACER function curve obtained from optimal curve fitting.

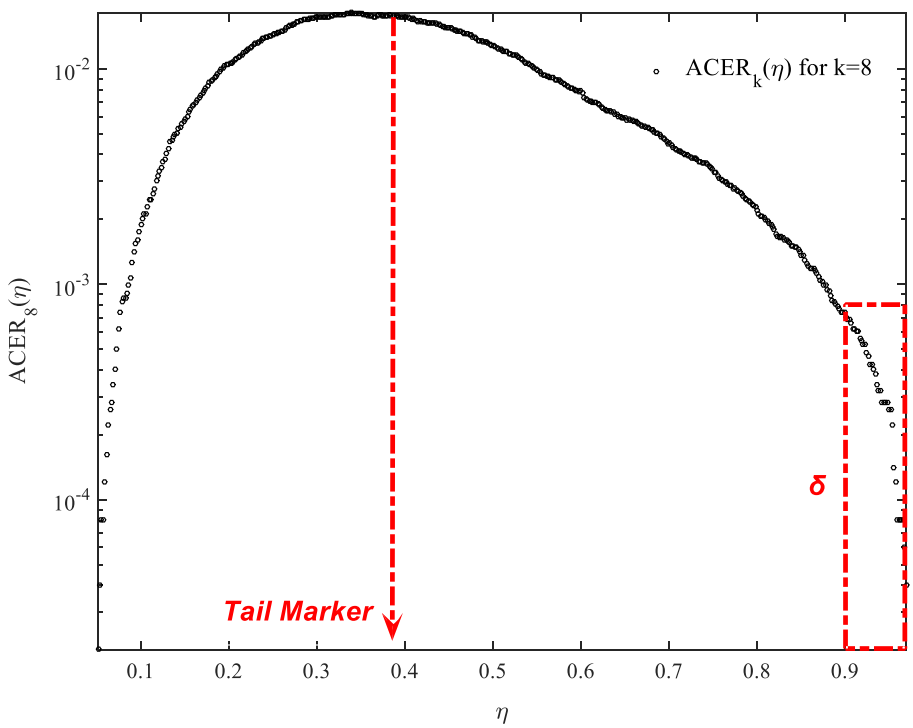

Fig. 9 Control of truncated points and uncertainty δ

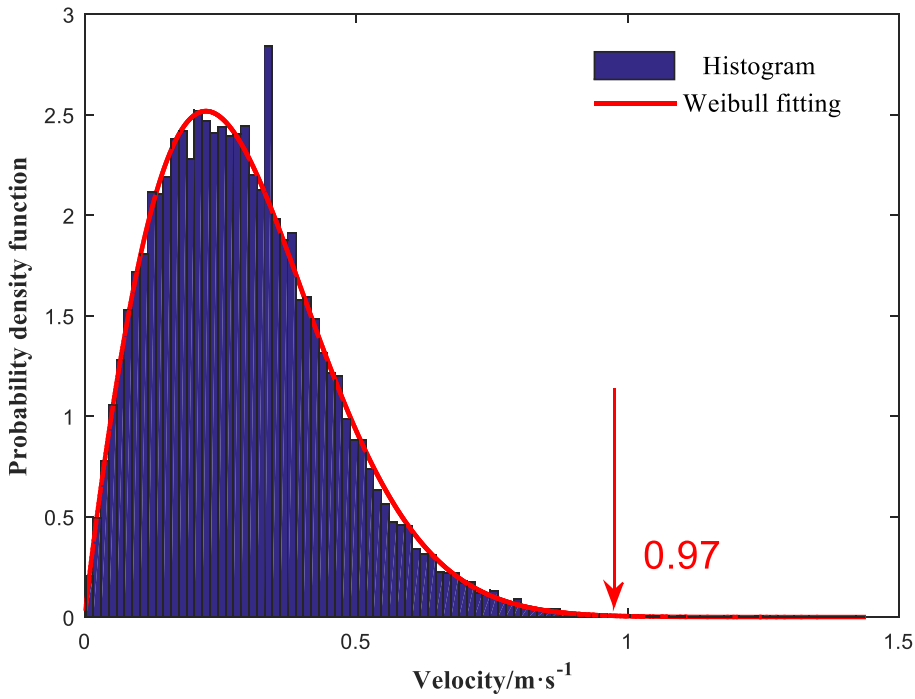

Fig. 10 Histogram auxiliary adjusting the uncertainty δ

4.2.3 Calculation of multi-year return period interval and comparisons of environmental design indexes

After optimal fitting of the curve, extrapolated predictions were conducted by the fitted curve on the recurrence interval of 1-year and 10-year for current profile in the LH11-1 sea area. The predictions with corresponding confidence intervals of current velocity for the 1st, 7th, and 14th layer for the 1-year return period are presented in Fig. 11-13. The optimal curve and confidence interval band are represented by a solid line and two dashed lines respectively. Though there are a few points in the tail part whose ACER function values are relatively small, those points with large uncertainties cannot determine the overall trend of the curve because the weighted least square method was adopted in the optimal fitting. In this way, we can find that the ACER algorithm tries to perform optimal fitting of ACER functions using a sufficient amount of data of relatively high precision to obtain reliable results. According to the calculation results shown in Fig. 11-13, the predicted current velocity results of the 1-year return period at the 1st, 7th and 14th layer are 1.22 m/s, 1.1 m/s, and 0.965 m/s, respectively.

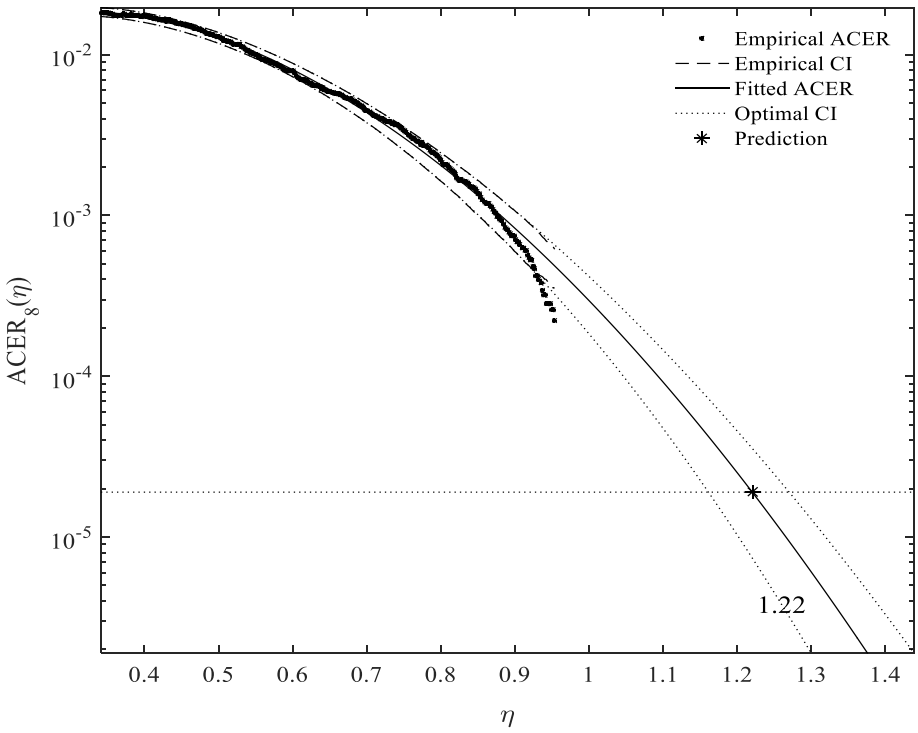

Fig. 11 Prediction value of current velocity of the 1st layer of the 1-year return period

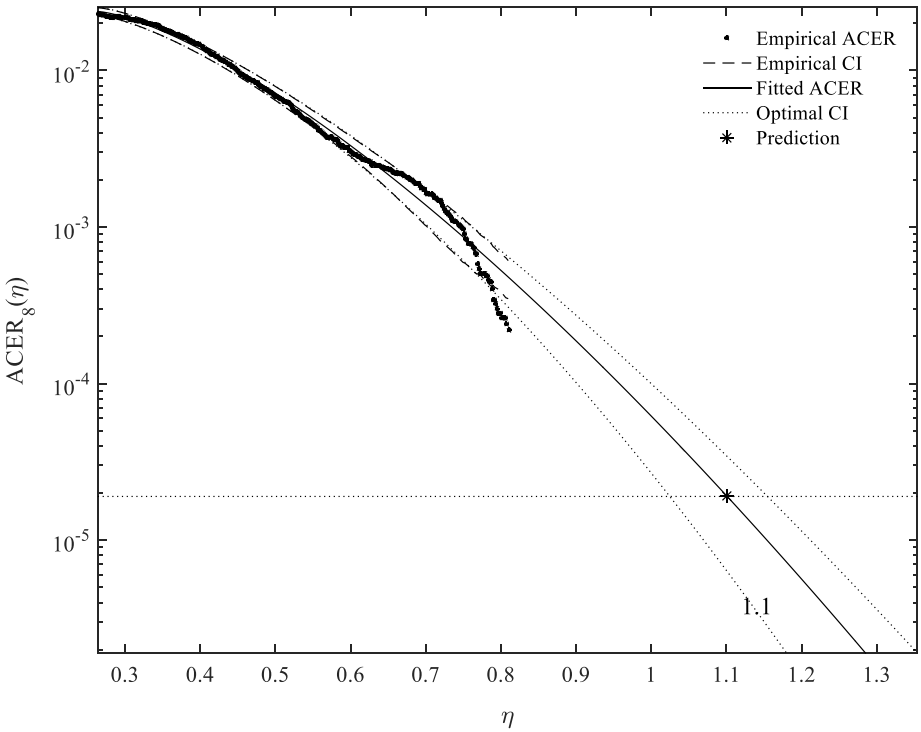

Fig. 12 Prediction value of current velocity of the 7th layer of the 1-year return period

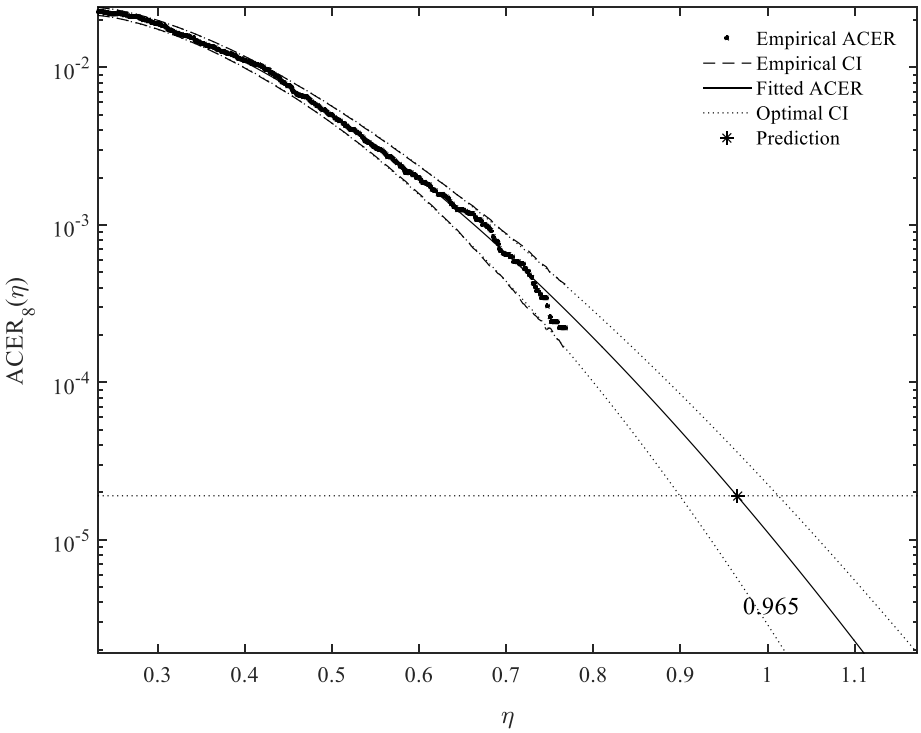

Fig. 13 Prediction value of current velocity of the 14th layer of 1-year return period

Prediction results (as shown in Fig. 14a, please see Table 1 for the detailed data) for multiyear return periods of the overall velocity profile indicates that the extreme value of current velocity under the given return period is similar to the hypothesized situation, where the current velocity is close to the shear flow. The overall trend of current velocity of the multiyear return period decreases as the depth increases, but the distribution curve is partially complex and zigzag. As a result, when the depth does not change greatly, the current velocity in the upper layer may be smaller than that of the lower layer.

At present, there are only a few floating platforms in South China Sea. The ocean environmental design indexes are different depending on the time of the design, even in the same sea area. Especially for early platform design, it is difficult to obtain the accurate ocean environmental design criteria without the effective in-situ monitoring data in the South China Sea.

Two current design indexes are selected to demonstrate the accuracy and feasibility of the ACER method in predicting the multi-year return values. Fig.14b and Fig.14c give the comparison of current profiles between the predicted results and the design indexes of two floating platforms both in same Liuhua sea area. Among the design indexes, “FPS” corresponds to a semisubmersible platform which design in 1980s, and “TLP” corresponds to a new design platform with sufficient ocean observational data.

Observing Fig. 14b and Fig. 14c (please see Table 2 and 3 for detailed data), the initial design index for FPS exhibited a large span of the velocity in depth. The profile of current velocity was simplified to such an extent that the current velocity of the initial design index in deep water was excessively underestimated with a large descending gradient observed in the 50 ~ 100 m depth layer for 1-year return values and 65~110m for 10-year return values. On the other hand, the variation of current velocity in the TLP design index is relatively smooth with depth, and is much closer to the predicted results. In spite of the fact that both design indexes of the upper layer for the 10-year return period were larger than the predicted values shown in Fig. 14c, the vast majority of the indexes for the TLP were located in the confidence band of predictions.

In conclusion, the difference between the two design indexes indicates that the early research on the extreme environmental conditions of the sea area was indeed not sufficient. Meanwhile, prototype monitoring technology has become an effective technical methodology. Predicted results via monitoring data and ACER show the consistency with the current design index of the TLP platform. Moreover，the present results in this paper reveal a more prominent advantage than the existing research on extreme current in the South China Sea. Firstly, the monitoring data is more reliable than the others which were mainly based on the numerical model or approximate estimation

by wind field and tide. Secondly, in terms of extreme value prediction method, the ACER method avoids artificial aspects of data sampling for the extreme value analysis and shows robustness and weak sensitivity to abnormal values. With the accumulation of monitoring data, the predicted results will continually refine and optimize the current design parameters.

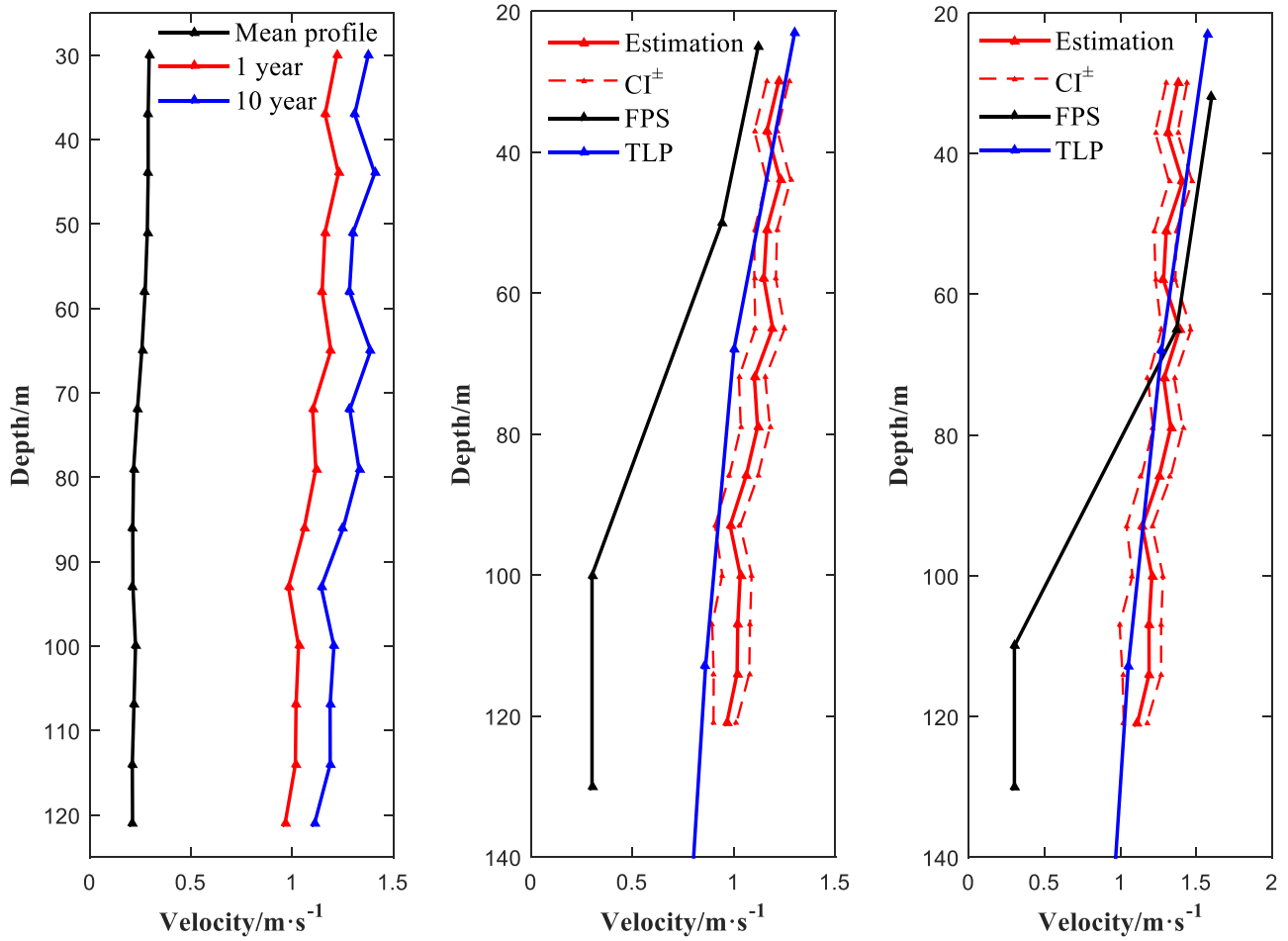

a. Return values by ACER method

b. Return value comparison in one-year

c. Return value comparison in 10 years

Fig. 14 Current profile distributions of return values for multiyear return period and comparison of ocean environmental design index in Liuhua sea area

Table 1 Predictions of current profile for multi-year return periods

Depth/m	Predictions of velocity for multi-year return periods（m/s）			
	1 Year		10 Year	
	Return values	95% CI	Return values	95% CI
30	1.22	(1.16,1.27)	1.38	(1.29,1.43)
37	1.16	(1.10,1.21)	1.31	(1.22,1.37)
44	1.23	(1.16,1.27)	1.41	(1.31,1.47)
51	1.16	(1.10,1.21)	1.30	(1.22,1.36)
58	1.15	(1.10,1.20)	1.28	(1.23,1.36)
65	1.19	(1.10,1.25)	1.39	(1.26,1.46)
72	1.10	(1.02,1.15)	1.28	(1.17,1.35)
79	1.12	(1.03,1.17)	1.33	(1.21,1.41)
86	1.06	(0.97,1.11)	1.25	(1.13,1.32)
93	0.98	(0.90,1.03)	1.14	(1.03,1.20)
100	1.03	(0.94,1.08)	1.21	(1.07,1.27)
107	1.02	(0.89,1.07)	1.19	(0.99,1.26)
114	1.02	(0.90,1.07)	1.19	(1.01,1.26)
121	0.96	(0.89,1.01)	1.11	(1.02,1.17)

Table 2 Design guides of current loads for SEMI FPS in Liuhua sea area

return period /Year	One		Ten	
current profile	D	V	D	V
	0	1.30	0	1.83
D=Depth (From	25	1.12	32	1.60
sea level，m),	50	0.94	65	1.37
V=Velocity(m/s)	100	0.30	110	0.30
	305	0.30	305	0.30

Table 3 Design guides of current loads for TLP platform in Liuhua sea area

return period /Year	One		Ten	
current profile	D	V	D	V
D=Depth (From sea level，m), V=Velocity(m/s)	0	1.46	0	1.73
	23	1.30	23	1.57
	68	1.00	68	1.27
	113	0.86	113	1.05
	159	0.76	159	0.91
	…	…	…	…

5. Conclusions

Profile analysis and prediction of extreme values of currents in the LH11-1 sea area were carried out based on actual data obtained by the prototype monitoring system of the NHTZ PFS. The main conclusions are presented as follows:

1) The measured velocity profile was relatively complex, presenting different forms and spatial shapes in different time periods with the main space shapes of shear flow. The current velocity in the middle layer was obviously less than that of other layers during some specific time periods;

2) For the mean current velocity profile, affected by small flow velocity of the middle layer as described above, it's difficult especially in the middle-lower layer to produce a complete shape of shear flow. And the middle layer showed an obvious trend of changes, where the current velocity decreased with depth with a large gradient.

3) The current velocity extreme profile in multiyear return periods was predicted with the ACER method. The results for one-year and decade return periods were obtained. To some extent, the spatial shapes were more or less similar for the extreme velocity profile and the mean profile. Overall, the upper current was stronger than the lower one, with partially tortuous profile shapes.

4) The comparison of predicted results with two design indexes showed that the current velocity determined by the existing design indexes of FPS has a large span of value varying with depth. The design index for FPS should be updated for practical engineering application. The design index for TLP is consistent with the predicted results by the ACER method.

The main purpose of this paper was to perform design verification in the LH11-1 area of the South China Sea, and aimed to provide beneficial guidance for load analysis, structural design, and production operation, based on the prototype measured data. To do this, a few typical space shapes and characteristics of the measured current profile were first analyzed. Then, a more accurate estimate for extreme current has been tried using the latest ACER extreme value analysis method. However, this present research is only a preliminary application of the measured data, and more extensive research and analysis approaches are still required. For example, the current univariate ACER method, like the other univariate extreme value methods, does not consider correlation between current layers, and how to consider the relevance of layered current to optimize existing results will be an important focus of future research.

In recent studies, some scholars have first applied a reduced dimensions method such as empirical orthogonal function to compress the data and reduce the variables before further analysis. In a future study, such kind of approaches will be incorporated with a multivariate extreme value methododology for an optimal design current profile of the South China Sea. Simultaneously, a

directional consideration will be introduced to determine the extreme characteristics of the current. Finally, combining spatial correlation and direction considerations, we hope to provide a current design criterion that is a fully three-dimensional design surface, rather than only the 2D profile generated by most research efforts. Thus, all the current extremal characteristics will be presented in 3D space. At present, part of the periodic work has been completed, and more results and details will be presented in future work. Overall, all the work aims at improving the problem of insufficient current specifications and the lack of effective reference data for engineering efforts in the South China Sea.

References

Carollo, C., Astin, I., & Graff, J. (2005). Vertical structure of extreme currents in the Faroe-bank channel. Annales Geophysicae, 23(6), 1977-1986.

Chen Shangji. (1991). Marine data processing analysis method and its application. The Ocean Publishing Company.

Dong Haijun. (2009). Application of Wind-driven Current Calculation in Return Period in Offshore. Port Engineering Technology, 46(2), 1-3.

Du Yu, Wu Wenhua, Yue Qianjin, Shi Zhongmin, Li Feng, & Xie Ribin, et al. (2016). Prototype Monitoring Technique for Deep Water Floating Platform. Journal of Shanghai Jiao Tong University, 50(3), 448-455.

Ewans, K., & Jonathan, P. (2014). Evaluating environmental joint extremes for the offshore industry using the conditional extremes model. Journal of Marine Systems, 130(1), 124-130.

Forristall, G.Z. & Cooper, C.K. (1997). Design Current Profiles Using Empirical Orthogonal Functions (EOF) and Inverse FORM Methods.

Ge Lili, Qu Yan, Zhang Zhixu, Yan Youfang, & Qi Yiquan. (2009).The calculation of the extreme wind, wave and current for return periods in the deep water area of the South China Sea. CHINA OFFSHORE OIL AND GAS, 21(3), 207-210.

Heffernan, J. E., & Tawn, J. A. (2004). A conditional approach for multivariate extreme values (with discussion). Journal of the Royal Statistical Society, 66(3), 497-546.

He Qi, Wei Zexun, & Wang Yonggang. (2012). Study on the sea currents in the northern shelf and slope of the South China Sea based on the observation. Acta Oceanologica Sinica, 34(1), 17-28

Jonathan, P., Ewans, K., & Flynn, J. (2012). Joint modelling of vertical profiles of large ocean currents. Ocean Engineering, 42(3), 195-204.

Jonathan, P., Flynn, J., & Ewans, K. (2010). Joint modelling of wave spectral parameters for extreme sea states. Ocean Engineering, 37(11-12), 1070-1080.

Karpa, O., & Naess, A. (2013). Extreme value statistics of wind speed data by the ACER method. Journal of Wind Engineering & Industrial Aerodynamics, 112(1), 1–10.

Lima, J.A.M., Ribeiro, E.O., Ceccopieri, W., Matheson, G.G., 2009. Directional Extreme Current Profiles Based on Complex Empirical Orthogonal Functions (C-EOF) for Offshore Design, ASME 2009 International Conference on Ocean, Offshore and Arctic Engineering, pp. 707-714.

Liu Yonggang, Yuan Yaochu, Liu Choteng, & Chen Hong. (2002). Measurement of the current and spectra analysis on the continental shelf in the East China Sea in June 1999. Acta Oceanologica Sinica (s1), 54-63.

Ma Qingshan. (2006). Regional frequency analysis of significant wave based on L-Moment. (Doctoral dissertation, Tianjin University).

Robinson, M.E., & Tawn J. A. (1997). Statistics for extreme sea currents. Appl. Statist., 46:183–205.

Naess, A., & Gaidai, O. (2008). Monte Carlo methods for estimating the extreme response of dynamical systems. Journal of Engineering Mechanics, 134(8), 628-636.

Naess, A., & Gaidai, O. (2009). Estimation of extreme values from sampled time series. Structural Safety, 31(4), 325-334.

Naess, A., Gaidai, O., & Batsevych, O. (2010). Prediction of extreme response statistics of narrow-band random vibrations. Journal of Engineering Mechanics, 136(3), 290-298.

Naess, A., Gaidai, O., & Teigen, P. S. (2007). Extreme response prediction for nonlinear floating offshore structures by Monte Carlo simulation. Applied Ocean Research, 29(4), 221-230.

Naess, A. & Karpa, O. (2015). Statistics of Extreme Wind Speeds and Wave Heights by the Bivariate ACER Method. Journal of Offshore Mechanics and Arctic Engineering. Transactions of the ASME, 137(2), 021602.

NDRC (National Development and Reform Commission). (2004). The specification of environmental conditions and environmental loads. China national offshore oil corporation enterprise standard（SY/T 10050-2004）.

Qu Yan, Du Yu, Wu Wenhua, Shi Zhongmin, & Yue Qianjin. (2013). Full scale measurement of LH11- 1 FPS hull and mooring system. The Ocean Engineering, 31(6), 1-8.

Skjong, M., Naess, A. & Brandrud Næss, O. E. (2013). Statistics of extreme sea levels for locations along the Norwegian coast. Journal of Coastal Research, 29(5), 1029-1048.

Smith, E. P. (2002). An introduction to statistical modeling of extreme values. Technometrics, 44(4), 107-111.

Veritas, D. N. (2000). DNV classification note - Environmental conditions and environmental loads. DNV NO.30.5, March 2000.

Wang Bin. (2005). The Distribution characteristics of extreme value of the Yellow and Bohai sea's marine hydrometeorological environmental. (Doctoral dissertation, Ocean University of China).

Wu Wenhua, Tang Da, Yue Qianjin, Shi Zhongmin, & QU Yan. (2013). Offshore platform structure prototype monitoring and its field application. Proceedings of the 16th China ocean (Coastal) engineering academic seminars (The upper part).

Yang Chenghao, Liao Guanghong, & Yuan Yaochu, et al. (2013). Structures of velocity profile in the Luzon Strait measured by ADCP in April 2008. Acta Oceanologica Sinica (in Chinese), 35(3), 1-10.

Yuan Shuangshuang. (2013). Prototype Measurement and Monitoring Technology Research of Floating Offshore Platform. (Doctoral dissertation, Dalian university of technology).